Contribution from the Department of Chemistry,
Texas A&M University, College Station, Texas 77843

Theoretical Study of the Dissociation of a Single Carbonyl from Chromium Hexacarbonyl

DAVID E. SHERWOOD, JR., and MICHAEL B. HALL*

Received March 1, 1982

Extended-basis-set Hartree–Fock–Roothaan calculations are reported for the dissociation of a single carbonyl ligand from chromium hexacarbonyl. As expected, the theoretical dissociation energy for the process $Cr(CO)_6 \rightarrow Cr(CO)_5 + CO$ (49.8 kcal mol^{-1}) is larger than the average dissociation energy (29.5 kcal mol^{-1}). The theoretical dissociation energy for the ion, $Cr(CO)_6^+ \rightarrow Cr(CO)_5^+ + CO$ (30.8 kcal mol^{-1}), agrees well with the recent mass spectral value (33.0 kcal mol^{-1}) of Michels, Flesch, and Svec (*Inorg. Chem.* **1980**, *19*, 479). Energy partitioning and analysis suggests that π bonding accounts for about 25% of the dissociation energy. Plots of the change in electron density as the carbonyl dissociates are reported. Comparison of these plots with those produced from various population analyses suggest that the σ bond involves primarily a rehybridization of the CO with little net transfer of electron density to the metal. The π bond, however, does involve a net transfer of charge from the metal to the carbonyl. Thus, the chromium is found to bear a net positive charge in agreement with the recent X-ray diffraction study of Rees and Mitschler (*J. Am. Chem. Soc.* **1976**, *98*, 7918). At very long chromium–carbon distances the carbonyl moiety may act like a "σ-only" ligand. Calculations of the change in the force between the C and the O of a free carbonyl as it approaches the $Cr(CO)_5$ fragment show that at moderately long Cr–C distances the force is such that the C–O bond distance should be shorter than that of free CO. A well-documented example of this is provided by the low-temperature X-ray structure of $Rh_2(O_2CCH_3)_4(CO)_2$ by Koh and Christoph (*J. Am. Chem. Soc.* **1979**, *101*, 1422). This molecule has a long Rh–C distance of 2.092 (4) Å and a remarkably short C–O distance of 1.120 (4) Å. Recently, Gagné et al. (*Inorg. Chem.* **1982**, *21*, 254) reported the structure of a Cu dimer that had C–O distances of 1.10 (1) and 1.11 (1) Å.

Introduction

Carbon monoxide bonds to a transition-metal center with a synergistic bond, which involves two distinct charge-transfer interactions. The first is σ donation of carbon "lone-pair" electron density to an empty metal d orbital; the second is π back-donation of metal "lone-pair" electron density to the 2π antibonding orbital of CO. The net effect is little or no net charge transfer between the carbonyl and the metal center. The capacity to bond and still remain electrically neutral gives the CO ligand its ability to stabilize transition-metal centers in low oxidation states. It is difficult experimentally to measure the magnitude of either charge-transfer interaction independently, and their relative importance is still being argued in the literature today.

Chromium hexacarbonyl has been extensively studied, both experimentally and theoretically, as a model system for transition-metal to carbon monoxide bonding. Even for this well-characterized system, there are conflicting interpretations of the role of π back-bonding. Klemperer and Johnson have recently reported the results of scattered-wave Xα (SW-Xα) calculations for $Cr(CO)_6$.[1] In their interpretation, σ donation from CO (CO $5\sigma \rightarrow$ Cr $3d_\sigma$) is the only important interaction for the metal–carbon bond, while π back-donation (Cr $3d_\pi \rightarrow$ CO 2π) strongly affects only the carbon–oxygen bond. This result is in apparent conflict with a number of molecular orbital (MO) studies.[2] Recently, Bursten and Fenske have projected the results from a similar SW-Xα calculation onto an atomic orbital basis set and have concluded that these calculations do indicate that π bonding is important for the chromium–carbon bond.[2e]

The σ-only bonding model was used by Klemperer and Johnson to interpret the ultraviolet absorption spectrum and low-energy photoelectron spectrum of $Cr(CO)_6$, which had previously been interpreted within a framework of extensive π back-bonding.[2] The strongest argument in favor of a σ-only model for the chromium–carbon bond is the trans influence found in the interaction coordinate analysis of Jones et al.,[3] where stretching a single Cr–C bond was found to affect only the trans Cr–C bond. We have recently shown[4] that the interaction coordinates can be semiquantitatively predicted within a framework of moderately strong π back-bonding using parameter-free Fenske–Hall MO calculations.[5]

In this study, we will examine the reaction (1) in detail, at

$$Cr(CO)_6 \rightarrow Cr(CO)_5 + CO \qquad (1)$$

several points along the dissociation curve, using Hartree–Fock–Roothaan (HFR)[6] calculations with a large basis set. Thus, we will examine the formation of the single, unique Cr–C bond and the perturbation of that unique carbonyl moiety. In addition, we will examine when CO can act as a "σ-only" donor and compare the electron density distributions and populations with experimental C–O bond lengths and stretching frequencies. Finally, the Cr–CO bond will be analyzed beyond the HFR level of calculation, with a limited configuration interaction (CI) approach.

Computational Details

All calculations at the HFR level were performed with the ATMOL3 program package[7] on a CDC 7600 computer at the Lawrence Berkeley Laboratory. Orbitals suitable for the CI calculation were optimized with the generalized molecular orbital (GMO) technique, which is described elsewhere,[8] and a CI calculation was performed among this optimized set.

The main limitation on performing HFR and CI calculations on large molecules such as $Cr(CO)_6$ is the time required for computation, which rapidly increases as the size of the basis set increases. A basis set was chosen specifically for describing the bond formation. For chromium the (12s) Gaussian set of Roos et al.[9] was modified[10] to

(1) Johnson, J. B.; Klemperer, W. G. *J. Am. Chem. Soc.* **1977**, *99*, 7132.
(2) (a) Hillier, I. H.; Saunders, V. R. *Mol. Phys.* **1971**, *22*, 1025. (b) Baerends, E. J.; Ros, P. *Ibid.* **1975**, *30*, 1735. (c) Caulton, K. G.; Fenske, R. F. *Inorg. Chem.* **1968**, *7*, 1273. (d) Beach, N. A.; Gray, H. B. *J. Am. Chem. Soc.* **1968**, *90*, 5713. (e) Bursten, B. E.; Freier, D. G.; Fenske, R. F. *Inorg. Chem.* **1980**, *19*, 1810.
(3) (a) Jones, L. H.; McDowell, R. S.; Goldblatt, M. *Inorg. Chem.* **1969**, *8*, 2349. (b) Jones, L. H. *J. Mol. Spectrosc.* **1970**, *36*, 398. (c) Jones, L. H.; Swanson, B. I. *Acc. Chem. Res.* **1976**, *9*, 128.
(4) Sherwood, D. E.; Hall, M. B. *Inorg. Chem.* **1980**, *19*, 1805.
(5) Fenske, R. F.; Hall, M. B. *Inorg. Chem.* **1972**, *11*, 768.
(6) Roothaan, C. C. *Rev. Mod. Phys.* **1951**, *23*, 69.
(7) Guest, M. F.; Hillier, I. H.; Saunders, V. R. "ATMOL3 System"; Daresbury Laboratory: Warrington WA4 4AD, U.K.
(8) (a) Hall, M. B. *Chem. Phys. Lett.* **1979**, *61*, 467. (b) Hall, M. B. *Int. J. Quantum Chem.* **1978**, *14*, 613. (c) Hall, M. B. *Int. J. Quantum Chem., Quantum Chem. Symp.* **1979**, *13*, 195.
(9) Roos, B.; Veillard, A.; Vinot, G. *Theor. Chim. Acta* **1971**, *20*, 1.

0020-1669/83/1322-0093$01.50/0

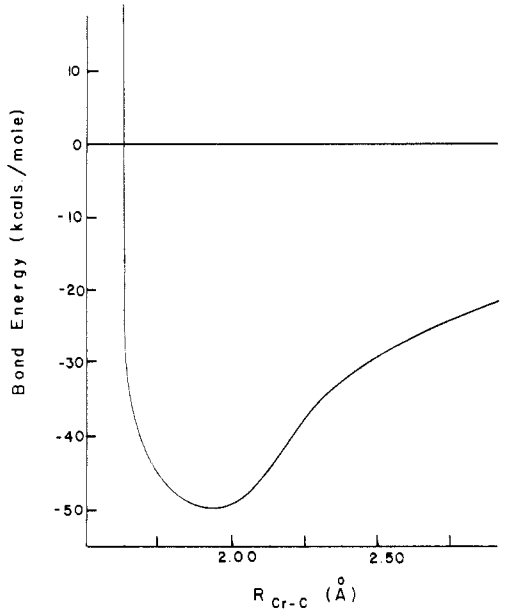

Figure 1. Qualitative potential energy curve for the dissociation of a single carbonyl from chromium hexacarbonyl.

make it more even-tempered and was contracted to [6s]. The (6p) Gaussian set of Roos et al.[9] was contracted to [3p], and two additional Gaussian functions were added (exponents 0.362 025 and 0.115 830) to form an even-tempered [5p]. The (6d) Gaussian basis set of Hay,[11] contracted to [3d], was used from the literature. This [6s, 5p, 3d] Gaussian basis set is large enough to give a good representation (better than double-ζ's for the valence electrons) of the Cr atom (39 atomic orbitals for 12 electron pairs). For the unique C and O, a (9s, 5p) Gaussian basis set was contracted to [4s, 2p],[12] which gives an adequate double-ζ (DZ) basis set (20 atomic orbitals for 7 electron pairs per CO group). All six carbonyl groups could not be represented by this DZ basis set due to size considerations. The other five carbonyl groups were described with the minimal [2s, 1p] contraction of the Gaussian (6s, 3p) basis set of Stewart[13] (10 atomic orbitals for 7 electron pairs per CO group). This approximation introduces an artificial asymmetry, such that the system will have C_{4v} symmetry at all points along the dissociation curve. However, the effect of this asymmetry is surprisingly small. The splitting of the t_{2g} eigenvalues is only 0.0087 au; the t_{2g} orbital populations differ by only 0.082 electron. In a very realistic sense these calculations represent the dissociation of CO from L_5CrCO, where Cr, C, and O are well represented and L is only a crude model for CO. Such an asymmetric basis set has successfully been used by Mitcheson and Hillier[14] to assign the satellite structure in the X-ray photoelectron spectrum of $Ni(CO)_4$.

Energetics of Dissociation of $Cr(CO)_6$

The geometry of $Cr(CO)_6$ was taken to be perfectly O_h, and the experimental values of Rees and Mitschler,[15] based on low-temperature X-ray diffraction, were used for the chromium–carbon bond distances (R_{Cr-C}) and the carbon–oxygen bond distances (R_{C-O}). To obtain the dissociation curve in Figure 1, we performed HFR calculations at several values of R_{Cr-C} for the unique carbonyl with the rest of the geometry frozen. The horizontal line in Figure 1 represents the total energy of the $Cr(CO)_5$ and CO fragments at infinite separation. Since one CO should dissociate properly from $Cr(CO)_6$ at the Hartree–Fock level, the dissociation curve shows a smooth approach to the dissociated fragments.

The calculated dissociation energy of one CO from the perfectly O_h geometry is 49.8 kcal mol^{-1}. This is substantially higher than the mean dissociation energy determined experimentally (29.5 ± 0.3 kcal mol^{-1}) by calorimetric methods.[16] Recent mass spectrometric work by Michels, Flesch, and Svec[17] on transition-metal carbonyls has shown that removing the first neutral CO from $Cr(CO)_6^+$ also takes more energy than the mean dissociation energy of $Cr(CO)_6^+$. On the basis of appearance potentials, loss of a single carbonyl from $Cr(CO)_6^+$ takes 33.0 ± 0.2 kcal mol^{-1} vs. the average dissociation energy of 26.7 ± 0.2 kcal mol^{-1} for

$$Cr(CO)_6^+ \rightarrow Cr^+ + 6CO \qquad (2)$$

Furthermore, we can compare our calculated dissociation energy, D_e(molecule), to that of the dissociation energy of the $Cr(CO)_6^+$ ion, D_e(ion), by using the relationship

$$D_e(\text{ion}) = D_e(\text{molecule}) - IP_{Cr(CO)_6} + IP_{Cr(CO)_5} \qquad (3)$$

where D_e is the energy for dissociating a single CO from the complex and IP is the ionization energy. If we make use of Koopmans' theorem, which states that the ionization potential is equal to the negative of the eigenvalue of the highest occupied molecular orbital,[18] we calculate a value of 30.8 kcal mol^{-1} for dissociating the first carbonyl from $Cr(CO)_6^+$. This value is in good agreement with the experimental value of 33.0 ± 0.2 kcal mol^{-1}.

There are several sources of error in our dissociation energy for $Cr(CO)_6$, which may have cancelled errors in the IP's to produce a fairly accurate dissociation energy for $Cr(CO)_6^+$. Because we have not allowed the separated fragments to relax their geometry and, hence, to lower their total energy relative to that of the united $Cr(CO)_6$ molecule, our dissociation energy may be too large. However, recent geometry studies by Lichtenberger and Brown[19] using Fenske–Hall calculations, and by Hay[20] using ab initio methods, have shown that the potential well for deforming $3d^6$ $M(CO)_5$ systems is extremely shallow. Thus, we expect the error due to the neglect of the geometry relaxation to be an order of magnitude smaller than the dissociation energy. Inadequacies in the basis set can produce an error in either direction. If we improved the basis set for Cr and the dissociating CO, the theoretical dissociation energy would probably increase. On the other hand, if we improved the basis set for the other five CO's, the theoretical dissociation energy would probably decrease. The latter error is probably more important. Again let us emphasize that this system should realistically be viewed as L_5CrCO, where L is only a crude model for CO. Our dissociation energy of 49.8 kcal mol^{-1} is quite reasonable for a system like L_5CrCO, where L is a somewhat poorer ligand than CO.

Analysis of the Dissociation Energy

In order to partition the energy of a molecule into component contributions, we must make some simplifying assumptions. We define a total electronic energy matrix, **E**, as

$$\mathbf{E} = \mathbf{D}(\mathbf{H} + \mathbf{DG}) \qquad (4)$$

where **D** is the density matrix, **H** is the one-electron energy matrix containing the kinetic energy and electron–nuclear attraction energy, and **G** is the two-electron energy matrix containing the electron–electron repulsions and Coulomb and

(10) The s functions with exponents of 0.094 109 and 0.036 848[9] were replaced with two tighter s functions having exponents of 0.188 218 and 0.073 696.
(11) Hay, P. J. *J. Chem. Phys.* **1977**, *66*.
(12) Dunning, T. H., Jr. *J. Chem. Phys.* **1971**, *55*, 2823.
(13) Stewart, R. F. *J. Chem. Phys.* **1969**, *50*, 2485.
(14) Mitcheson, G. R.; Hillier, I. H. *J. Chem. Soc., Faraday Trans. 2* **1979**, *75*, 929.
(15) Rees, B.; Mitschler, A. *J. Am. Chem. Soc.* **1976**, *98*, 7918.
(16) Skinner, H. A. *Adv. Organomet. Chem.* **1964**, *2*, 49.
(17) Michels, G. D.; Flesch, G. D.; Svec, H. J. *Inorg. Chem.* **1980**, *19*, 479.
(18) Koopmans, T. *Physica (Amsterdam)* **1933**, *1*, 104. Our theoretical IP's are 10.05 eV for $Cr(CO)_6$ and 9.23 eV for $Cr(CO)_5$. These values are both too large due to errors in Koopmans' theorem, but their difference should be free of these errors.
(19) Lichtenberger, D. L.; Brown, T. L. *J. Am. Chem. Soc.* **1978**, *100*, 366.
(20) Hay, P. J. *J. Am. Chem. Soc.* **1978**, *100*, 2411.

Table I. Energy Analysis of the Dissociation of One Carbonyl from $Cr(CO)_6$[a]

energy[b]	$Cr(CO)_6$	$Cr(CO)_5 + CO$	$Cr(CO)_6 - (Cr(CO)_5 + CO)$
$E_{elec}(\sigma)$	−2320.558 22	−2161.433 63	−159.124 59
$E_{elec}(\pi)$	−370.079 71	−319.417 96	−50.661 75
E_{elec}	−2690.637 93	−2480.851 59	−209.786 34
E_{NR}	982.061 09	772.354 12	209.706 97
E_{tot}	−1708.576 84	−1708.497 47	−0.079 37

[a] Energies are in atomic units. [b] See text for definitions of energy terms.

exchange integrals. The total electronic energy is the trace of this energy matrix

$$E_{elec} = \sum_{i=1}^{k} E_{ii} \quad (5)$$

where the sum is over all basis functions. The simplest separation of the energy is to consider the contribution of each basis-set orbital in eq 5 to the total electronic energy. Due to the high symmetry of both the united $Cr(CO)_6$ molecule and the $Cr(CO)_5$ and CO fragments, the atomic orbitals can be separated into a σ set (orbitals lying along the internuclear axis) and a π set (orbitals with nodes along the internuclear axis). The change in the total electronic energy can, therefore, be examined with respect to σ and π contributions. Each orbital energy term, however, contains higher order two-electron contributions including σ–π cross terms which we will not attempt to analyze independently in this study. The total energy of a molecule, E_{tot}, is defined as

$$E_{tot} = E_{elec} + E_{NR} \quad (6)$$

where E_{NR} are the nuclear–nuclear repulsions. The energy terms in Table I demonstrate the magnitude of the numbers involved. The change in total energy between the united $Cr(CO)_6$ molecule and the $Cr(CO)_5$ and CO fragments must be divided into two parts: the change in nuclear–nuclear repulsions, which are large and positive, and changes in electronic energy, which are large and negative. These two contributions cancel to give a relatively small negative number, the dissociation energy. In the following discussion we will not try to analyze the dissociation energy itself, but we will simply partition the rather large electronic energy, E_{elec}. However, because of the rather arbitrary nature of all partitioning schemes, the results should be interpreted as suggestive rather than definitive.

We assume that the $2p_\pi$ orbitals of the carbonyl groups have only pure π energy contributions and neglect possible σ interactions with cis carbonyl groups. This assumption is supported by the small density elements found between cis carbonyl $2p_\pi$ atomic orbitals. All of the metal p orbitals were included as σ energy contributors. We find that, of the total electronic energy change on formation of the united $Cr(CO)_6$ molecule, 24.1% is gained by π type orbitals (Table I). This substantial percentage is in direct conflict with the findings of Klemperer and Johnson,[1] who maintain that the Cr–C bond in $Cr(CO)_6$ can be described as a σ-only bond. One can further divide the σ orbital set into what are classically considered to be core (i.e., C 1s; O 1s; Cr 1s, 2s, 2p, 3s, 3p) and valence (i.e., C 2s, 2p; O 2s, 2p; Cr 3d, 4s, 4p). The core electronic energy gain is 39.3% of the total, and the σ valence electronic energy gain is 36.5% of the total. Hence, considering only the valence energy lowering between the united $Cr(CO)_6$ molecule and the $Cr(CO)_5$ and CO fragments, the σ and π contributions are nearly equal.

Since the molecular orbitals of the $Cr(CO)_5$ and CO fragments can also easily be divided into σ and π type MO's, the change in total energy was also examined as a sum over fragment orbitals. This involves only a simple basis-set transformation using the fragment vectors and fragment overlap matrix.[21] This has one advantage over the atomic orbital basis set, in that the Cr p orbitals will be more correctly accounted for. Some small Cr p character is used in Cr–CO π bonding, and the fragment orbitals will have this Cr p_π bonding built in. The π contribution in this analysis of the difference in total electronic energy upon bond formation is 25.8%, a result that is slightly higher than the result from the atomic orbital analysis. Both analyses are consistent and indicate a substantial π contribution to the formation of the chromium–carbon bond in $Cr(CO)_6$.

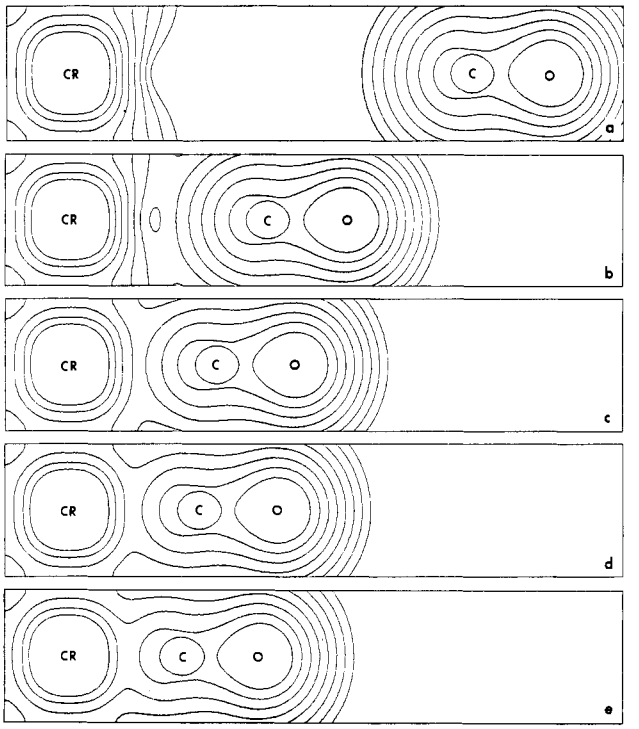

Figure 2. Total electron density plotted for several points along the dissociation curve shown in Figure 1. The chromium–carbon bond distances are as follows: (a) infinite separation plotted 4.0 Å apart; (b) 1.0 Å longer than the equilibrium distance; (c) 0.25 Å longer than the equilibrium distance; (d) the equilibrium separation; and (e) 0.25 Å shorter than the equilibrium distance. There are eight contours, which increase by a multiplicative factor of 2.0 from the lowest contour, which represents 0.039 062 5 electron/cubic atomic unit.

Density Changes along the Dissociation Curve

Total electron density maps at several points along the dissociation curve are shown in Figure 2. The fragments' geometries have been frozen, and only the displacement of the CO moiety from its O_h equilibrium position, ΔR_{Cr-C}, has been varied. The map of the fragments' densities at infinite separation was plotted at the nuclear positions corresponding to a Cr–C distance 4.0 Å longer than the experimental distance (Figure 2a). The map in Figure 2b is the density of a $Cr(CO)_6$ molecule with the unique chromium–carbon bond stretched 1.0 Å. Similarly, Figure 2c corresponds to a 0.25-Å stretch, Figure 2d is the O_h geometry, and Figure 2e is a 0.25-Å chromium–carbon bond compression.

The separated fragments map, Figure 2a, shows that the $Cr(CO)_5$ fragment in square-pyramidal geometry has a region of low density in the direction of the incoming CO. This represents an electron density "picture" of a vacant coordination site. In a sense, the $Cr(CO)_5$ fragment density is prepared to receive an electron donor. As we have fixed the geometry of $Cr(CO)_5$, this vacant site may be more analogous

(21) Hall, M. B. Ph.D. Thesis, University of Wisconsin, 1971.

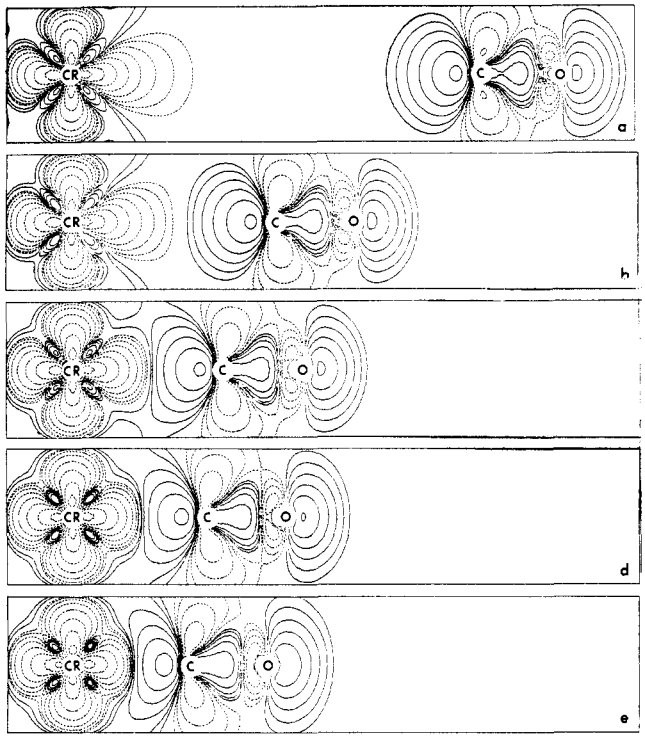

Figure 3. Atomic deformation densities plotted for several points along the dissociation curve in Figure 1. The geometries and contour values are identical with those of Figure 2. Solid contours denote electron density gain, and dashed contours denote electron density loss.

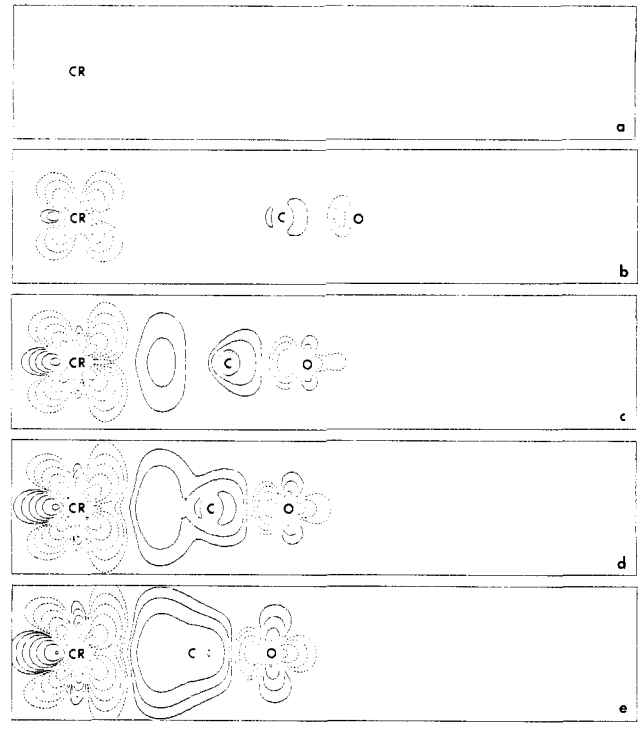

Figure 4. Fragment deformation densities plotted for several points along the dissociation curve in Figure 1. The geometries and contour values are identical with those of Figure 2. Solid contours denote electron density gain and dashed contours denote electron density loss.

to a coordinatively unsaturated site on a surface than it is to a true $Cr(CO)_5$ site. When the CO moiety is brought closer, very little change can be discerned in the total densities (Figure 2b–e), since the change in electron density upon bond formation is only a small perturbation of the total fragment electron density.

Atomic deformation density maps (Figure 3) were calculated as the total density of the molecule minus that of the neutral spherical atoms (Cr = $[Ar]3d^54s^1$, ^7S; C = $[He]2s^22p^2$, ^3P; O = $[He]2s^22p^4$, ^3P), at the same geometry. Solid contours represent density gain, and dashed contours represent density loss. Since the total deformation density must integrate to zero, these maps represent a redistribution of electron density when the atoms form bonds. Both σ and π changes can be seen in the regions off the internuclear axis, but only σ changes can be seen along the internuclear axis. The deformation densities of the separated fragments, $Cr(CO)_5$ and CO, are shown in Figure 3a. The carbonyl molecule shows a buildup of density in the C and O lone pair regions. There is a buildup of electron density along the carbon–oxygen internuclear axis and a concurrent shift of $2p_\pi$ density from the atoms to the bond region. These shifts are consistent with the formation of multiple bonds in the CO moiety. For the $Cr(CO)_5$ fragment, we are concerned with the Cr region and the effect of the five CO ligands that disturb the Cr electron density. The symmetry of the $Cr(CO)_5$ fragment is formally C_{4v}, and the occupied metal orbitals are the same $3d_\pi$ orbitals that would be occupied in $Cr(CO)_6$. The spherical Cr atom has one electron in each of the five 3d orbitals and one electron in the Cr 4s orbital. This corresponds roughly to a $3d_\pi^3 3d_\sigma^2 4s^1$ configuration. In the $Cr(CO)_5$ molecule the configuration of the Cr atom is closer to $3d_\pi^6 3d_\sigma^0 4s^0$. The $3d_\sigma$ orbitals are destabilized by CO $5\sigma \rightarrow 3d_\sigma$ donation from the five CO ligands. The $3d_\pi$ orbitals are stabilized by $3d_\pi \rightarrow$ CO 2π back-donation and become strongly occupied. Thus, when the spherical Cr atom is subtracted, we see a loss in $3d_\sigma$ density along the internuclear axis and a gain of $3d_\pi$ density in the regions off the internuclear axis.

As the CO moiety is brought closer (Figure 3b–e), we observe only small changes in the atomic deformation density. Most of the changes in the maps involve only slight distortions of the shapes of contours in the region of the O "lone pair" and of the C–O bond. Between the Cr and C atoms there is a cancellation of the C "lone-pair" gain and the $Cr(CO)_5$ $3d_\sigma$ loss as the fragments are brought together. The zero-density region, where the C loss and the Cr gain exactly cancel, moves from the C side toward the midpoint of the Cr–C bond, indicating net movement of some C "lone-pair" density into the interbond region. As with the total densities, the atom deformation densities obscure the density changes that are unique to the chromium–carbonyl bond formation. The maps are dominated by the formation of C "lone pairs", O "lone-pairs", and C–O bonding and by the Cr atomic arrangement.

Fragment deformation density maps were calculated as the total molecular densities minus the densities of the neutral $Cr(CO)_5$ and CO molecules at the same internuclear distances as the molecular totals (Figure 4). This series of maps shows the electron density changes for one CO molecule bonding to a $Cr(CO)_5$ fragment. The map of the fragments at infinite separation (Figure 4a) is zero everywhere. As the ligand approaches the $Cr(CO)_5$ fragment, we begin to see slight changes in the CO σ framework at a Cr–C distance about 1.0 Å longer than the equilibrium bond length (Figure 4b). Hence, even at this long M–C distance, CO is beginning to act as a "σ donor". Concurrently, there is a change in electron density distribution about the Cr atom, which responds to the approaching CO electron density even at a large distance (Figure 4b). The most strongly affected orbitals are the two Cr $3d_\pi$ orbitals which are suitable for π bonding with the incoming CO. Although the approaching CO is still too far from the Cr to have π interactions, these two Cr $3d_\pi$ orbitals interact strongly with the one trans and four cis carbonyls. The incoming CO σ density causes the Cr to donate more π-electron density to the five carbonyls in the $Cr(CO)_5$ fragment. This is seen as negative lobes off the internuclear axis in the shape of a Cr $3d_\pi$ orbital. As a consequence, the five carbonyls,

which are now electron rich, become better σ donors. The map with the 1.0-Å displacement of the incoming CO from its O_h equilibrium position shows an increase in σ electron density trans to this CO. At smaller displacements (Figure 4c–e) we begin to see Cr $3d_\sigma$ gain in the cis directions, but the trans gain is always larger. The σ and π changes on the Cr atom reflect the synergistic nature of the chromium–carbonyl bonds.

As we bring the CO in closer, we see a buildup of π density on the O atom, which begins to occur at about 0.25 Å longer than the equilibrium bond length (Figure 4c). Only at this shorter distance does CO begin to act as a "π acceptor". The Cr $3d_\pi$ loss becomes noticeably asymmetric because the $Cr(CO)_5$ fragment is now acting as a π donor to the incoming CO. There is an increased rearrangement of the incoming CO's σ density and a buildup of charge in the Cr–C bond region. Only near the O and Cr atoms are the σ and π density changes easily separable. The Cr–C bond region and the C atom region are positive everywhere and are both σ and π in nature. As we bring the incoming CO even closer (Figure 4d,e), all of the interactions increase and density changes become larger but remain qualitatively the same.

The buildup of electron density between the Cr and C atoms in the interbond region moves slightly toward the Cr atom as the CO is brought in. The overall changes upon bond formation are (1) a reorganization of CO σ density, which forces more of the CO "lone-pair" density into the interbond region and (2) a gradual increase in π density on the CO ligand and loss of Cr $3d_\pi$ density about the chromium center, a change that is consistent with Cr $3d_\pi \rightarrow$ CO 2π back-donation. The σ interaction, as described, is not totally a charge-transfer interaction. If we examine the Cr atom region, we do not find a large gain in the $3d_\sigma$ orbital that is pointing toward the incoming CO. Undoubtedly, some component of σ charge transfer exists, but near the Cr atom it is overwhelmed by the Cr $3d_\pi$ donation. Thus, the Cr atom should have a slight positive charge. The "lone pair" on the C atom has been pushed out slightly toward the Cr, which would make the C atom positive, but the direct Cr $3d_\pi \rightarrow$ C $2p_\pi$ donation makes the C nearly neutral. The O atom also receives some net negative charge from the Cr $3d_\pi$ donation. The σ rearrangement, which leads to density loss near the oxygen atom, is confined to the region of the internuclear axis, whereas the π gain is more diffuse and actually joins the C atom at contours that have values too small to be shown in Figure 4. This diffuse π gain, which extends quite far away from the oxygen atom, gives the oxygen atom an overall negative charge. The net charge transfer, $Cr(CO)_5 \rightarrow CO$, is consistent with the experimental charge distribution found by Jolly,[22] who used X-ray photoelectron spectroscopy, and by Rees and Mitschler,[15] who integrated the experimental electron density.

Our total molecular densities and atomic deformation densities at the equilibrium geometry are qualitatively similar to those found in the X-ray diffraction study of Rees and Mitschler[15] and the theoretical study of Heijser et al.[23] However, our fragment analysis is different from either of these studies. Rees and Mitschler subtracted six CO's and a Cr atom in a $t_{2g}^{3.8}e_g^{1.2}4s^{1.0}$ configuration. Their C–O regions look the same as ours, but the regions between the Cr and C atoms are negative everywhere except for a slight buildup at the midpoint of the bond. Heijser subtracted six CO's and a Cr atom in a $t_{2g}^{6}e_g^{0}4s^{0}$ configuration. His map shows a loss of density on the C atoms and a large gain of electron density in the Cr $3d_\sigma$ orbitals. Our calculation provides an additional point of view, that of the formation of a single Cr–C bond in the $Cr(CO)_6$ molecule. The converged $Cr(CO)_5$ fragment has a density distribution similar to that of the united $Cr(CO)_6$ molecule about the Cr center, and the effects of the other five Cr–C bonds are minimized in the fragment deformation density maps. In summary, when joining the $Cr(CO)_5$ and CO fragments together to form the unique Cr–C bond, we see a buildup of electron density in the Cr–C interbond region and concurrent Cr $3d_\pi \rightarrow$ CO 2π charge transfer.

Population Analysis

The molecular and deformation densities, which are displayed in the previous maps, are representations of the true density, derived within the limits of the calculation performed. Discussions of such maps are qualitative, however, because so many functions make a contribution to any given point on the map. In order to discuss interactions and charge transfer between orbitals, it is necessary to first look at the true density matrix, D_{ij}, for n doubly occupied orbitals, defined as

$$D_{ij} = 2\sum_{l}^{n} C_{il}C_{jl} \tag{7}$$

where C_{il} and C_{jl} are the coefficients of the ith and jth basis function in the lth molecular orbital. The fragment orbital basis set can be used to study the effect of individual fragment orbitals upon bond formation such as the CO 5σ and 2π orbitals, which are classically considered in carbonyl σ donation and π acceptance. For two fragments, A and B, we can partition the density matrix for the molecule into three parts: D_{AA}, D_{BB} diagonal terms, D_{AB} interaction terms, and $D_{AA'}$, $D_{BB'}$ internal rearrangement terms. The diagonal terms plus the interaction terms integrate to the total number of electrons and represent directly the charge transfer among fragment orbitals. The internal rearrangement terms integrate to zero, but they do redistribute the electron density. The fragments at infinite separation have a density matrix with no off-diagonal terms in the fragment orbital basis set. The diagonal terms are either 2.0 for a doubly occupied molecular orbital or 0.0 for a virtual orbital. The change in electron density upon bond formation, $\Delta\mathbf{D}$, is a matrix defined as

$$\Delta\mathbf{D} = \mathbf{D}_{\text{molecule}} - \mathbf{D}_{\text{fragments}} \tag{8}$$

Since the fragment density matrix is diagonal, only the diagonal part of the molecular density matrix is affected. There are several problems in analyzing $\Delta\mathbf{D}$ directly. First, there are $\sim k^2/2$ terms, where k is the number of basis functions. Second, the interaction terms are functions centered between fragments and hence are not a simple change in fragment density. Third, the diagonal terms of $\Delta\mathbf{D}$ do not add up to zero, although $\Delta\mathbf{D}$ integrates to zero.

It is traditional to use orbital populations to describe the bonding between atoms and fragments. They are convenient because there are only k terms, where k is the number of basis functions, and they sum to the total number of electrons. Most population schemes use the overlap matrix, $\mathbf{S}$, to distribute the diagonal and interaction density elements into orbital populations. Since populations are only an approximation for the calculated density, we have used two different population analyses.[24] With the fragment orbital basis set, any population scheme for the fragments at infinite separation gives a population of 2.0 for an occupied orbital and 0.0 for a virtual orbital (since both the eigenvectors and the overlap matrix are the unit matrix). Thus, the orbital populations for the fragments at infinite separation represent the true calculated density. The change in a fragment orbital population, ΔP_i, should reflect density changes upon bond formation

$$\Delta P_i = P_{i_{\text{molecule}}} - P_{i_{\text{fragment}}} \tag{9}$$

subject to limitations of the approximations involved in forming

(22) Jolly, W. L.; Avanzino, S. C.; Reitz, R. R. *Inorg. Chem.* **1977**, *16*, 964.
(23) Heijser, W. Ph.D. Thesis, Vrije Universiteit te Amsterdam, 1979.
(24) (a) Mulliken, R. S. *J. Chem. Phys.* **1955**, *23*, 1841. (b) Löwdin, P. O. *Ibid.* **1950**, *18*, 365.

Table II. Population Analysis for $(CO)_5Cr$–CO Bond Formation

	$\Delta 5\sigma$	$\Delta 2\pi$	$\Delta\sigma_{tot}$[a]	$\Delta\pi_{tot}$[a]
Mulliken	−0.23340	0.15342	−0.22016	0.08758
Löwdin	−0.61542	0.43590	−0.51312	0.45124

[a] The total change is given as the change for the sum over all orbitals of a symmetry type.

the fragment orbital populations for the united molecule.

The Mulliken population of a fragment orbital in a molecule is given by

$$P_i^M = 2\sum_l^n \sum_j^k C_{il}C_{jl}S_{ij} \tag{10}$$

where the off-diagonal elements of the density matrix are partitioned equally between the two orbitals involved. This scheme can lead to orbital populations greater than 2.0 and less than 0.0. The Löwdin populations are taken as the diagonal elements of the Löwdin density matrix obtained from

$$P_i^L = (S^{+1/2}DS)_{ii} \tag{11}$$

While the orbitals on fragment A are orthogonal and the orbitals on fragment B are orthogonal, they are not orthogonal to each other. The Löwdin analysis orthogonalizes the two fragment basis sets to each other and creates a new set of totally orthogonal fragment orbitals that are most like the original fragment orbitals in a least-squares sense. Thus, the Löwdin populations and the change in Löwdin populations on formation of the molecule are for new orbitals that are extremely similar to the fragment orbitals. The Löwdin populations are still positive and have values $0 \leq P_i^L \leq 2.0$.

The changes in Mulliken and Löwdin populations upon bond formation for the unique CO moiety are given in Table II. Both schemes show donation from the 5σ orbital. If we add up all the contributions from the σ orbitals of CO, $\Delta\sigma_{tot}$, we find a net donation of −0.22 from the CO to the $Cr(CO)_5$ fragments. This is in agreement with the classical description of CO $\sigma \rightarrow$ Cr $3d_\sigma$ donation. Both schemes show donation from the Cr $3d_\pi$ orbitals to the 2π orbitals. The sum of all the π contributions, $\Delta\pi_{tot}$, is +0.09. Thus, both schemes show a larger CO σ donation than CO π acceptance, but the net amount of charge transfer is small. The Löwdin populations show much greater individual changes but give a more neutral CO.

The population analysis supports the classical charge-transfer "picture" of metal–carbonyl bonding, but do the changes in populations reflect the true density changes as shown in the density plots? We can examine this question by calculating the density of the molecule implied by the populations and subtracting the fragment densities. Figure 5a shows a plot of the Löwdin population changes. Here we see a loss of σ density about the C atom and a large Cr $3d_\sigma$ gain. The Cr $3d_\pi$ donation to the CO moiety is large; the O π gain is obscured by the large O $2p_\sigma$ loss. The plot of the Mulliken population changes (Figure 5b) is similar but does not show a gain in Cr $3d_\sigma$ density and shows a gain only at the O end of the CO moiety. Neither map looks like that shown in Figure 4d.

There are two reasons why the population changes do not mirror the density changes upon bond formation. First, the approximation that partitions the D_{AB} interaction terms may not do so correctly. Second, any population scheme will not include the internal rearrangement terms, since $S_{AA'}$ and $S_{BB'}$ are equal to zero for eq 10 and 11. Although these internal rearrangements or rehybridization terms integrate to zero in the $\Delta\mathbf{D}$ matrix, they redistribute the electron density. If, for instance, we add the internal rearrangements to the change in Mulliken populations, we get a buildup of charge in the Cr–C bond region (Figure 5c). This result indicates that the

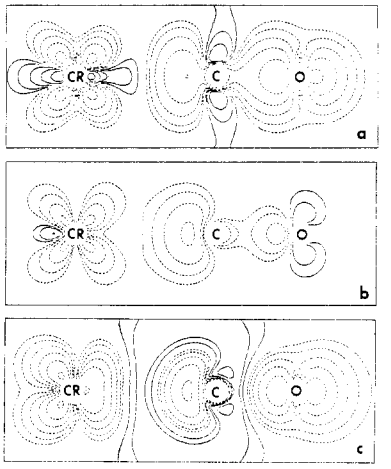

Figure 5. Changes in populations, which occur on the formation of $Cr(CO)_6$ from the fragments $Cr(CO)_5$ and CO, plotted (a) for the Löwdin populations, (b) for the Mulliken populations, and (c) for the Mulliken populations corrected for fragment orbital rehybridization. The contour values are identical with those in Figure 2. Solid contours denote electron density gain, and dashed contours denote electron density loss.

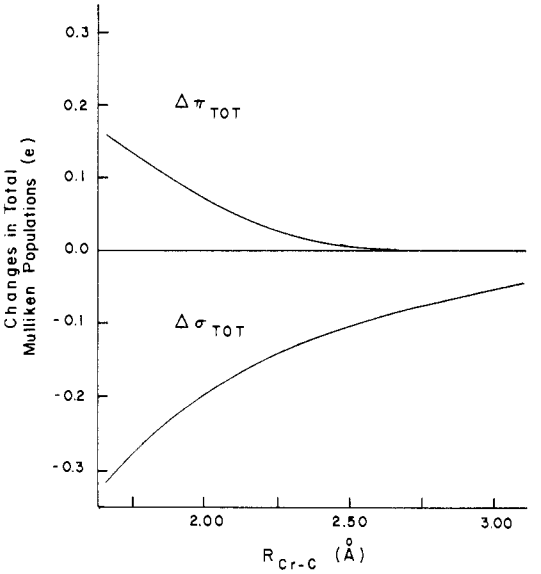

Figure 6. Total changes in the Mulliken populations for the unique carbonyl plotted as a function of the chromium–carbon bond length.

buildup of charge between the Cr and C atoms is, to some extent, due to the rehybridization of the fragment orbitals allowing the C "lone pair" of CO to expand into the interbond region, rather than a direct charge transfer to the Cr atom. Even with these additional terms, the map still shows an exaggerated σ loss close to the C nucleus and in the O $2p_\sigma$ region. Thus, the corrected population map still does not quantitatively reflect the density changes, but it does show reduced C $\sigma \rightarrow$ Cr $3d_\sigma$ charge transfer, which is exaggerated in the simple population analysis. The corrected Löwdin population map (not shown) is similar. Thus, the populations, which seem to satisfy the classical idea of the donor–acceptor bond, do not even correctly account for the charge transfer in the true electron density.

Although the populations fail to correctly represent the electron density, trends in their values may still be useful. The changes in Mulliken populations are sensitive to Cr–C distance and both the $\Delta\sigma_{tot}$ and $\Delta\pi_{tot}$ go to zero at infinite separation, i.e., dissociated CO. Figure 6 shows a plot of these values, relative to free CO, as a function of chromium–carbon distance. The $\Delta\pi_{tot}$ curve is smaller in absolute value and falls

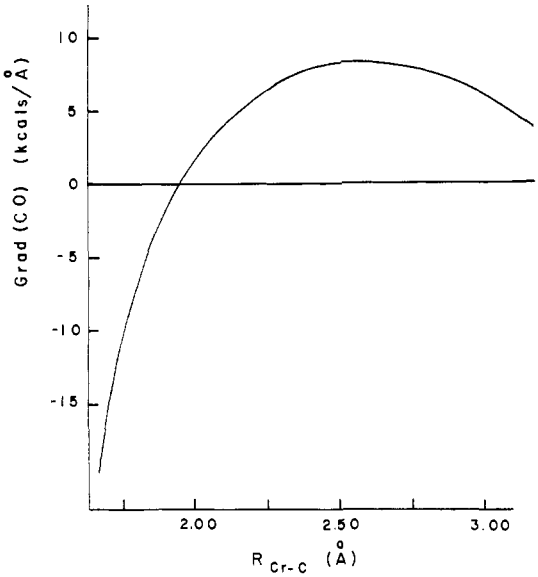

Figure 7. Gradient of the unique carbonyl (the force on the C–O bond) plotted as a function of the chromium–carbon distance. Negative values indicate a longer C–O bond, and positive values indicate a shorter C–O bond. Zero corresponds to free CO.

off much more rapidly than the $\Delta\sigma_{tot}$ curve. This is consistent with the smaller overlap of the Cr–C π bonds relative to the Cr–C σ bonds. As in the previous discussions of the fragment deformation density as a function of R_{Cr-C}, this result suggest that at very long Cr–C bond distances CO can act in a "σ-only" fashion.

Dependence of R_{C-O} on R_{Cr-C}

As we have seen in the previous discussion of electron density and populations, changes in the σ electrons begin at extremely long Cr–C distances. Since the 5σ orbital is slightly antibonding,[25] carbonyl 5σ donation should strengthen the C–O bond. In the absence of Cr d_π to carbonyl 2π back-bonding, which normally dominates carbon–oxygen bond strength, the CO bond at long Cr–C distances should become stronger than that of free CO. Such a situation exists in certain ionic metal–carbonyl complexes where the metal is not a strong π donor. For example, Ozin's matrix-isolated complexes of gold[26] and silver[27] and DeKock's[28] $(CO)MF_2$ (M = Cr, Mn, Co, Ni, Zn) complexes all exhibit higher stretching frequencies (ν_{CO}) than that of free CO.

In order to determine the relationship between R_{C-O} and R_{Cr-C}, we have calculated the force on the C–O bond at several points along the $(CO)_5Cr-CO$ dissociation curve. First R_{C-O} of free CO was optimized in the [4s,2p] basis with the HONDO program.[29] Then, we performed two calculations for each point on the dissociation curve, alternately stretching and compressing the CO bond 0.01 Å about the optimized value of 1.137 905 Å. The gradient, grad(CO), was calculated as the difference in total energy of stretched and compressed configurations divided by ΔR_{C-O} (0.02 Å). Figure 7 shows a plot of grad(CO) vs. R_{Cr-C}. Negative values indicate a lengthening of the CO bond; positive values indicate a shortening of the CO bond. At short and normal Cr–C bond lengths, the CO bond length is predicted to be longer than that of free CO (negative grad(CO)) as is observed in $Cr(CO)_6$ and most of the transition-metal compounds. The negative grad(CO) also suggests a weaker CO bond, and most transition-metal complexes show stretching frequencies below that of free CO. At long Cr–C bond lengths the gradient becomes positive and the CO bond length is predicted to be shorter than that of free CO. Our calculations evaluate grad(CO), which is the force that contracts or lengthens the CO bond. They do not predict how much the CO distance will change, but previous work suggests that the range of CO distances is small.[30] Direct evidence from X-ray crystal structures for these small changes in R_{C-O} with R_{M-C} must, therefore, be viewed with careful consideration of the accuracy of experimental measurement. For one class of rhodium–carbonyl complexes, Koh's plot of R_{C-O} vs. R_{M-C}[31] has the general shape of our gradient curve, but only in a few compounds, notably $Rh_2(O_2CCH_3)_4(CO)_2$[32] and $RhCl(CO)(P(t\text{-}Bu)_3)_2$,[33] is R_{C-O} significantly shorter than that of free CO. These compounds have extremely long Rh–C bond lengths as we would expect from our theoretical results. A recently reported copper dimer has C–O distances of 1.10 (1) and 1.11 (1) Å with Cu–C distances of 1.809 (7) and 1.781 (7) Å, respectively.[34]

To evaluate the CO stretching frequencies as a function of R_{Cr-C} would have taken several more calculations at each point along the dissociation curve. We believe that a plot of ν_{CO} vs. R_{Cr-C} would have the same shape as our gradient curve, but it would be displaced toward larger values of R_{Cr-C}. Thus, it should be easier to stretch a CO bond even at long metal–carbon distances if the metal is a good π donor. At moderately long M–C distances the CO bond becomes shorter than that of free CO but the stretching frequency may still be lower than that of free CO. The rhodium and copper compounds mentioned above fall into this category. At extremely long M–C distances or with very poor π donors the CO bond should be shorter and the stretching frequency should be higher than those of free CO. This is the case in the highly oxidized species discussed previously. Assuming the shape of the ν_{CO} vs. R_{M-C} curve is the same as our gradient curve, we can estimate the magnitude of $\Delta\nu_{CO}$. In the short and normal R_{M-C} range, where the slope is steep, $\Delta\nu_{CO}$ will be large and negative, while in the long R_{M-C} range, $\Delta\nu_{CO}$ will be small and positive. Most carbonyl complexes show substantial frequency lowering, while in the few complexes that have a ν_{CO} greater than that of free CO, it is only slightly greater.

Configuration Interaction

So far, we have limited our discussion to results derived within the HFR approximation. It is possible that electron correlation could drastically alter the description and properties of the electronic structure. In order to explore this question, we performed a limited CI calculation on $Cr(CO)_6$ with the atoms located at their O_h equilibrium positions. In the GMO orbital optimization and subsequent CI only six MO's were considered: the σ-bonding orbital and the two π-bonding orbitals and their antibonding counterparts. These molecular orbitals are plotted in Figure 8 in order of increasing orbital energy. The Cr–C σ bond (Figure 8d) is predominantly CO 5σ in character with some chromium p_σ and d_σ character. The CO is bonding with the Cr $4p_\sigma$ orbital, which, because of orthonormality considerations, mixes in some Cr $3p_\sigma$ antibonding character. This produces an internal node which is near the Cr atom. The Cr–C σ^* orbital (Figure 8a) is predominantly Cr $3d_\sigma$ representing the formally empty $3d_\sigma$ orbital

(25) Hall, M. B.; Fenske, R. F. *Inorg. Chem.* **1972**, *11*, 1619.
(26) Huber, H.; McIntosh, D.; Ozin, G. A. *Inorg. Chem.* **1977**, *16*, 975.
(27) Huber, H.; Ozin, G. A. *Inorg. Chem.* **1977**, *16*, 64.
(28) DeKock, C. W.; Van Liersburd, D. A. *J. Am. Chem. Soc.* **1972**, *94*, 3235; *J. Phys. Chem.* **1974**, *78*, 134.
(29) (a) DuPuis, M.; King, H. F. *J. Chem. Phys.* **1978**, *68*, 3998. (b) McIver, J. W.; Komornicki, A. *J. Am. Chem. Soc.* **1972**, *94*, 2625.
(30) Cotton, F. A.; Wing, R. M. *Inorg. Chem.* **1965**, *4*, 314.
(31) Koh, Y. B. Ph.D. Thesis, The Ohio State University, 1979.
(32) Koh, Y. B.; Christoph, G. G. *J. Am. Chem. Soc.* **1979**, *101*, 1422.
(33) Shumann, H.; Heisler, M.; Pickart, J. *Chem. Ber.* **1977**, *110*, 1020. This structure may have unrefined disorder.
(34) Gagné, R. R.; Kreh, R. P.; Dodge, J. A.; Marsh, R. E.; McCool, M. *Inorg. Chem.* **1982**, *21*, 254.

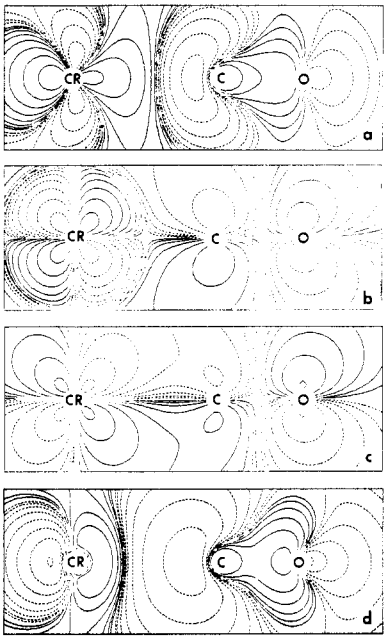

Figure 8. Plot of the GMO orbitals involved in the Cr–CO bond and used in the configuration interaction calculation. The contour values are the same as those of Figure 2 but denote the amplitude of the molecular orbitals.

in O_h symmetry. This orbital is antibonding between the Cr $3d_\sigma$ and CO 5σ orbital, and the node now appears in the interbond region. The Cr–C π-bonding orbitals (one is shown in Figure 8c) are predominantly Cr $3d_\pi$ orbitals with some 2π CO character. The Cr–C π^* antibonding orbitals (one is shown in Figure 8b) are predominantly CO 2π orbitals with a small antibonding contribution from the metal d orbitals.

In the CI calculation all paired double excitations between these orbitals were considered. The resultant CI wave function for $Cr(CO)_6$, although not accurate enough for quantitative results, can be used to show the effect on the electronic structure when one begins to include electron correlation. The final natural orbital configuration is $\sigma^{1.99}\pi^{3.85}\pi^{*0.15}\sigma^{*0.01}$. The leading configuration is the HFR ground state (97%). This result indicates the HFR ground state is already a good qualitative representation for the electron structure of $Cr(CO)_6$. The most important CI contribution is $\pi^2 \rightarrow \pi^{*2}$, which increases the charge transfer from the Cr $3d_\pi$ orbitals to the CO 2π orbitals. The CI calculations allow the π electron on the chromium atom to spend more time on the CO moiety, thereby reducing the electron–electron repulsions. The σ excitations yield only minor contributions to the CI wave function. Thus, the near-degenerate electron correlation is mostly π in nature. These results indicate that π bonding is at least as important as it appears in the HFR approximation and that the importance of π bonding will not be diminished by the use of more sophisticated molecular orbital techniques. Recent analysis of Auger line shapes in metal carbonyls provides some direct evidence that the charge distribution obtained from HFR calculations is essentially correct.[35]

Acknowledgment. The authors gratefully acknowledge the support of the National Science Foundation (Grant No. CHE 79-20993) and of the National Resource for Computation in Chemistry under a grant from the National Science Foundation (Grant No. CHE 77-21305) and the Basic Energy Sciences Division of the U.S. Department of Energy (Grant No. W-7405-ENG-48).

Registry No. $Cr(CO)_6$, 13007-92-6.

(35) Jennison, D. R.; Stucky, G. D.; Rye, R. R.; Kelber, J. A. *Phys. Rev. Lett.* **1981**, *46*, 911.

Contribution from the Department of Chemistry, Brooklyn College, City University of New York, Brooklyn, New York 11210, and Department of Science, John Jay College of Criminal Justice, City University of New York, New York, New York 10019

SO_2···HF. An ab Initio Study

MARVIN E. FRIEDLANDER, JAMES M. HOWELL,* and ANNE-MARIE SAPSE*

Received January 8, 1982

STO-3G and extended basis set calculations were performed on the complex formed between SO_2 and HF. The most stable geometry (−5.2 kcal/mol relative to the noninteracting molecules) was found, as expected, to be with the HF linear to the S–O bond with a separation of 1.8 Å. Calculations of the electric field potential surrounding the SO_2 were also performed.

During the past several years, much work has been done in the field of hydrogen bonding. Recently, it has been shown that molecular orbital calculations done within the Hartree–Fock approximation agree excellently with results of high-resolution spectroscopy.[1-4] Although some work has been done on hydrogen-bonded sulfur-containing systems,[5] none as yet has dealt with sulfur dioxide.

We focused our attention on the interaction between the SO_2 and the HF molecules, with the former as a proton acceptor and the latter as a proton donor. This system is of interest due to the presence of SO_2 in atmosphere in concentrations of 0.2 ppb, where it forms clusters with negative ions such as NO_3^-, Cl^-, and others. These clusters exhibit high binding energies and have been extensively studied by experimental methods. It is advanced that SO_2 binds to the negative ions even more strongly than water and, as such, can affect the negative ion content of the atmosphere.[6] Electrostatic interactions play a crucial part in the formation of the clusters, and it seems worthwhile to investigate the SO_2 ability to form various types of bonds with other molecules. The case of the interaction with HF is of specific interest since it allows us to look also at different aspects of hydrogen-bond formation.

* To whom correspondence should be addressed: J.M.H., Brooklyn College; A.-M.S., John Jay College of Criminal Justice.

(1) H. Popkie, H. Kistenmacher, and E. Clementi, *J. Chem. Phys.*, **59**, 1325 (1973).
(2) D. Hankins, J. W. Moskowitz, and F. H. Stillinger, *J. Chem. Phys.*, **53**, 4544 (1970).
(3) L. A. Curtiss and J. A. Pople, *J. Mol. Spectrosc.*, **48**, 413 (1973).
(4) G. H. F. Diercksen, *Theor. Chim. Acta*, **21**, 335 (1971).
(5) J. R. Sabin, *J. Chem. Phys.*, **54**, 4675 (1971); *J. Am. Chem. Soc.*, **93**, 6291 (1971).
(6) F. E. Fehsenfeld and E. E. Ferguson, *J. Chem. Phys.*, **61**, 5181 (1974).

0020-1669/83/1322-0100$01.50/0